Acoustic centering of sources measured by surrounding spherical microphone arrays

Ilan Ben Hagai[a)]
Department of Electrical and Computer Engineering, Ben-Gurion University of the Negev, Beer-Sheva 84105, Israel

Martin Pollow and Michael Vorländer
Institute of Technical Acoustics, RWTH Aachen University, D-52056 Aachen, Germany

Boaz Rafaely
Department of Electrical and Computer Engineering, Ben-Gurion University of the Negev, Beer-Sheva 84105, Israel

(Received 16 February 2011; revised 24 July 2011; accepted 25 July 2011)

The radiation patterns of acoustic sources have great significance in a wide range of applications, such as measuring the directivity of loudspeakers and investigating the radiation of musical instruments for auralization. Recently, surrounding spherical microphone arrays have been studied for sound field analysis, facilitating measurement of the pressure around a sphere and the computation of the spherical harmonics spectrum of the sound source. However, the sound radiation pattern may be affected by the location of the source inside the microphone array, which is an undesirable property when aiming to characterize source radiation in a unique manner. This paper presents a theoretical analysis of the spherical harmonics spectrum of spatially translated sources and defines four measures for the misalignment of the acoustic center of a radiating source. Optimization is used to promote optimal alignment based on the proposed measures and the errors caused by numerical and array-order limitations are investigated. This methodology is examined using both simulated and experimental data in order to investigate the performance and limitations of the different alignment methods. © *2011 Acoustical Society of America*. [DOI: 10.1121/1.3624825]

PACS number(s): 43.60.Fg, 43.38.Md [AJZ] Pages: 2003–2015

I. INTRODUCTION

The radiation pattern is an important characteristic of a sound source, representing the sound directivity and spatial propagation of the acoustic waves. The study of the radiation pattern is important for auralization, when one is interested in reproducing sound fields of musical instruments using an array of loudspeakers,[1] and therefore an accurate measurement of the instrument performance is of importance. Another application of the study of radiation patterns of acoustic sources is for the purpose of noise reduction of a noisy machine using active control of sound,[2] where the information about the machine sound directivity is used for reducing the noise emission. Furthermore, analyzing and modeling the acoustic radiation pattern of a human speaker is useful for measurement techniques of microphones used in telephones[3] and enables the simulation of the mouth as a complex sound source rather than a simple omnidirectional source.[4] This is important in applications dealing with the measurement of intelligibility parameters that are affected by the directivity of the source, such as the speech transmission index in cars.

Directivity measurements of musical instruments and human voice have been performed using various methods of microphone placement around the sources. For example, (1) measuring the directivity of a singer using a linear array of microphones,[5] (2) measuring the directivity of musical instruments recording using two circular arrays of microphones, one vertical and one horizontal,[6] and (3) measuring the sound directivity of a violin using a horizontal circular array and shifting the array in the vertical plane to achieve sampling on a cylindrical surface.[7] Directivity measurements using a spherical array of microphones have been performed using 12 microphones and then reproduced using electronic string instruments.[8] Similar measurements were carried out using an array of 32 microphones in a full anechoic chamber in order to investigate the sound directivity of a large number of instruments.[9] Another work[10] described a setup of 64 spherically arranged microphones. The spherical arrays, as opposed to arrays used in previous studies, provided complete directional information on the radiated sound field that was only limited by the total number of microphones used to capture the sound field.

Sound field analysis of acoustic sources using spherical microphone arrays has been performed previously in several ways. One option is by using a full sphere of fixed-position microphones.[11] Other options include the placement of a hemisphere of microphones surrounding the source from the upper side,[12] or the rotation of a single microphone using a scanning system.[13] After sampling the sound pressure, the sound directivity can be represented by spherical harmonics, which is an efficient tool for the analysis and reproduction of sound.[14] The maximal order of the spherical harmonics

[a)]Author to whom correspondence should be addressed. Electronic mail: ilanbe@bgu.ac.il

representation is determined by the number of microphones employed and therefore the desired spatial resolution can be controlled.[11]

Although previous studies of sound field measurement and analysis presented useful methods for characterizing the directivities of sound sources, most of these studies did not consider variations in the directional pattern due to variations in source positioning. Reference 9 suggested that a displacement in the source position may affect the measured radiation pattern. Variations in source position may occur due to both source rotation and source translation. In the case of measurement and analysis using spherical arrays, rotational changes of a sound field can be easily handled due to the spherical symmetry of these arrays; this is because the amplitudes of the spherical harmonics coefficients are modified only within a given order n, and can be rotated back by a simple multiplication with the rotation Wigner-D matrix in the spherical harmonics domain.[15] Therefore, when one is interested in investigating the directional pattern of a sound source, a certain flexibility in the source angular position is afforded. However, radiation directivity is highly sensitive to coordinate translation. For example, consider a point source located at the origin and radiating a perfect spherical wave that is represented by a single spherical harmonic of order zero. Higher orders will soon appear when the point source is shifted away from the origin.[16]

It is therefore important to overcome variations in the representation of sound radiation due to translation. The acoustic center of a sound source, which is determined by the center of the spherical waves, measured at some distance away from the source[17,18] can be used for this.

Most of the literature regarding the acoustic center is focused on sources with known sound radiation functions[17–19] so that the acoustic center is determined in these cases using analytically closed forms. The acoustic center of microphones, speakers, and human ears has been studied using models.[18] An important property of the acoustic center is that it does not necessarily coincide with the source location.[20] This was demonstrated using measurements and a computer model of a horn by examining changes in the nulls angles as a function of frequency.

Recently, acoustic alignment algorithms have been applied to measured directivity data of musical instruments.[21] Another method has been suggested to determine the acoustic center and to compensate for movement of measured sources and presented an algorithm for the alignment of sources measured by spherical microphone arrays using spherical harmonics.[22] This method facilitates compensation for changes in the radiation pattern due to displacement as well as providing a more efficient representation for spatial encoding purposes.

This paper expands on the published work of Rafaely[22] and presents a comprehensive error analysis that determines the limitations of this method as well as an examination of the algorithm using simulation studies and an experimental investigation using recorded data. The effect of source translation on the radiation pattern and on its spherical harmonics representation is investigated. The translation operator is developed both analytically and numerically, and an analysis of the error generated by sampling and translation is presented. Several measures for locating the acoustic center of a source captured with a surrounding microphone array are proposed.

The aforementioned method is investigated for sources of low directivity such as monopoles and musical instruments playing at low frequencies and succeeds in aligning such sources for the purposes of compensation for spatial deviation and of efficient spherical harmonics representation for spatial encoding. However, for sources of high directivity, as well as sources radiating at high frequencies, the results of this method are generally not as good in terms of repeatability and convergence to the physical center, which limits the frequency and directivity range that the algorithm can handle with satisfactory results.

This paper offers the following contributions:

(1) Development of a method for the centering of measured acoustic sources.
(2) Presentation of a comprehensive error analysis for sampling and translation of sources represented with spherical harmonics expansions.
(3) Presentation of simulation results illustrating the performance and limitations of the method.
(4) Demonstration of an experimental study of the method using recorded data.

II. SOUND FIELD REPRESENTATION BY SPHERICAL HARMONICS

Source alignment, as applied in this paper, is based on spherical harmonics decomposition. Therefore, a description of the spherical harmonics and the exterior problem in spherical coordinates is now introduced, based on the work of Williams.[16] A sound pressure in space is denoted by $p(k, r, \theta, \varphi)$, where k is the wave number and (r, θ, φ) are the standard spherical coordinates.[23] Consider such a pressure field which is square integrable on the unit sphere, radiating from a source bounded by a sphere of radius a. Then the radiated pressure field is given by

$$p(k,r,\theta,\phi) = \sum_{n=0}^{\infty} \sum_{m=-n}^{n} c_{nm}(k) h_n(kr) Y_n^m(\theta,\phi), \tag{1}$$

where $h_n(kr)$ are the spherical Hankel functions of the first kind, c_{nm} are the coefficients that support the equation, and the spherical harmonics $Y_n^m(\cdot,\cdot)$ are defined by

$$Y_n^m(\theta,\phi) \equiv \sqrt{\frac{(2n+1)}{4\pi}\frac{(n-m)!}{(n+m)!}} P_n^m(\cos\theta) e^{im\phi}, \tag{2}$$

where n is the order of the spherical harmonics, $P_n^m(\cdot)$ is the associated Legendre function, and $i = \sqrt{-1}$. The coefficients c_{nm} can be computed using the orthogonality of the spherical harmonics around the unit sphere. Multiplying Eq. (1) with the complex conjugate of the spherical harmonics on both sides and integrating the result around the unit sphere gives

$$c_{nm}(k) = \frac{1}{h_n(kr)} \int_{S^2} p(k, r, \theta, \phi) Y_n^m(\theta, \phi)^* d\Omega, \quad (3)$$

with $d\Omega = \sin\theta \, d\theta \, d\phi$ and the asterisk denoting the complex conjugate. Having found $c_{nm}(k)$, the pressure function can be computed using Eq. (1) at every point satisfying $r > a$.

The above-presented derivation suggests that knowledge of the sound pressure on a sphere can be used to compute the pressure at every point outside the sphere through the coefficients c_{nm}. Note that the sound fields considered in this paper are harmonic over time, such that $p(k, r, \theta, \varphi, t) = p(k, r, \theta, \varphi)e^{-i\omega t}$, where ω is the angular frequency and t represents time.[16]

III. SOUND FIELD SAMPLING

In this section, the theory of sampling and reconstruction of the sound field is presented. The aim is to compute coefficients c_{nm} using samples from the sound field, rather than the continuous function. This is the case in practice when data are recorded by spherical microphone arrays.

Consider a sound field in space, in which all sound sources are bounded by a sphere. The sound field can be represented as an infinite summation using Eq. (1). If the sound field is assumed to be order-limited, and coefficients c_{nm} in Eq. (1) are zero for all $n > N$, then the sum can be truncated as follows:

$$p(k, r, \theta, \phi) = \sum_{n=0}^{N} \sum_{m=-n}^{n} c_{nm}(k) h_n(kr) Y_n^m(\theta, \phi). \quad (4)$$

The pressure at a set of Q positions in space is denoted by the $Q \times 1$ vector $\mathbf{p}$,

$$\mathbf{p} = \left[p(r_1, \theta_1, \phi_1), p(r_2, \theta_2, \phi_2), \ldots, p(r_Q, \theta_Q, \phi_Q)\right]^T. \quad (5)$$

We have omitted the dependence on k for notation simplicity. Using Eq. (4), $\mathbf{p}$ can be represented by the following matrix equation:

$$\mathbf{p} = \mathbf{H}\mathbf{c}, \quad (6)$$

where $\mathbf{c}$ is the coefficient vector of size $(N+1)^2 \times 1$,

$$\mathbf{c} = \left[c_{00}, c_{1(-1)}, c_{10}, c_{11}, \ldots, c_{NN}\right]^T, \quad (7)$$

and $\mathbf{H}$ is a matrix of size $Q \times (N+1)^2$, which includes the Hankel function multiplying the spherical harmonics defined by $\mathbf{H} = [\mathbf{h}_1, \mathbf{h}_2, \ldots, \mathbf{h}_Q]^T$, where

$$\mathbf{h}_q = [h_0(kr_q)Y_0^0, h_1(kr_q)Y_1^{-1}, h_1(kr_q)Y_1^0 \; h_1(kr_q)Y_1^1, h_2(kr_q)Y_2^{-2}, \ldots, h_N(kr_q)Y_N^N]^T, \quad (8)$$

We have omitted the dependence of the spherical harmonics Y_n^m on (θ_q, ϕ_q) for notation simplicity. Equation (6) can be solved in a least-squares sense in order to find $\mathbf{c}$,

$$\mathbf{c} = \mathbf{H}^\dagger \mathbf{p}, \quad (9)$$

where $\mathbf{H}^\dagger$ is an $(N+1)^2 \times Q$ matrix represented by the Moore–Penrose pseudoinverse of $\mathbf{H}$. We assume that $Q > (N+1)^2$, so that oversampling of the sound field is employed, and that matrix $\mathbf{H}$ is well-conditioned. If matrix $\mathbf{H}$ is ill-conditioned, a large numerical error may occur, causing inaccurate values for $\mathbf{c}$, as discussed in detail in Sec. VI.

Because the sound field is uniquely determined by Eq. (4), calculating the coefficients vector using Eq. (9) enables the calculation of the pressure function at every point in the space outside of a sphere that contains all sources, under the assumption that the field is order-limited.

IV. TRANSLATED SOUND PRESSURE

In this section, we present the spherical harmonics representation under coordinate system translation. The theory presented in this section is used later in this paper for the development and analysis of the alignment methods. Consider a fixed constellation of a source with unknown acoustic center and a spherical observation of its sound radiation that surrounds the source at a constant radius $r = a$. After a coordinate system translation by $\mathbf{r}''$, the above-presented constellation is shifted to $-\mathbf{r}''$, as illustrated schematically in Fig. 1. In the new coordinate system, the spherical sound pressure observation is no longer belonging to points of a constant coordinate $r' \neq a$. Using Eq. (4), and omitting the dependence on k, the sound field before the translation can be written as

$$p(\mathbf{r}) = \sum_{n=0}^{N} \sum_{m=-n}^{n} c_{nm} h_n(kr) Y_n^m(\theta, \phi), \quad (10)$$

where in this case $\mathbf{r} = (a, \theta, \phi)$.

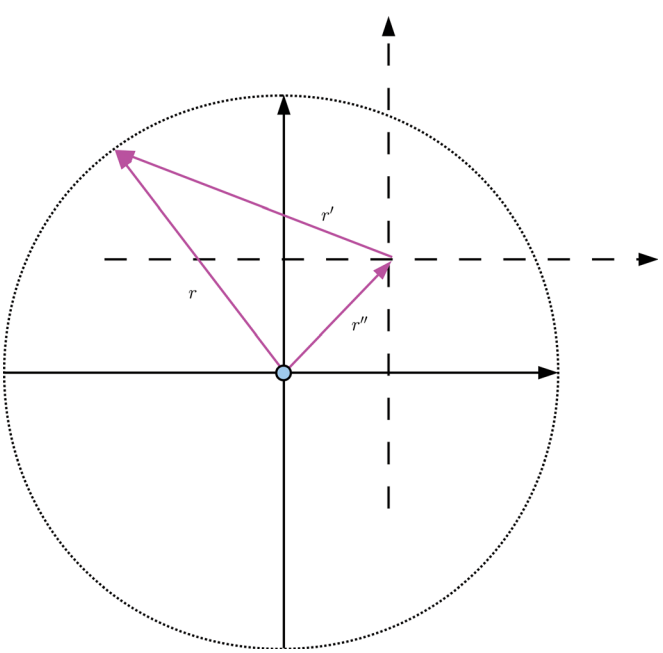

FIG. 1. (Color online) Linear translation in a spherical coordinate system.

We now investigate the effect of translation. The sound field on the sphere surface before and after the translation remains the same, but the coordinates of the points on the sphere surface are changed due to the coordinate system translation, as illustrated in Fig. 1. Equation (4) for the translated coordinate system now becomes

$$p'(\mathbf{r}') = \sum_{n=0}^{N} \sum_{m=-n}^{n} c'_{nm} h_n(kr') Y_n^m(\theta', \phi'), \tag{11}$$

with $\mathbf{r}' = (r', \theta', \phi')$. It is emphasized that the decomposition of the sound field with respect to the shifted origin in terms of c'_{nm} is not necessarily order-limited, and truncation errors may appear, as discussed in Sec. VI. Equations (10) and (11) are equated and are written in a matrix form as

$$\mathbf{p} = \mathbf{H}'\mathbf{c}' = \mathbf{H}\mathbf{c}. \tag{12}$$

Multiplying from the left by $\mathbf{H}'^{\dagger}$ gives the relation between the decomposed spherical harmonic coefficients in the original coordinate system and at the translated ones,

$$\mathbf{c}' = \mathbf{H}'^{\dagger}\mathbf{H}\mathbf{c}. \tag{13}$$

That is, the relation between $\mathbf{c}$ in the original coordinate system, and $\mathbf{c}'$ in the translated coordinate system, is given by a transformation matrix $\mathbf{T}$ as

$$\mathbf{T} = \mathbf{H}'^{\dagger}\mathbf{H}. \tag{14}$$

V. ANALYTICAL REPRESENTATION OF TRANSLATION

The numerical approach described in Sec. IV provides an expression for the transformation matrix $\mathbf{T}$ relating the spherical decomposition coefficients in the original and in the translated coordinate systems. This section derives the same transformation matrix analytically, based on the work of Chew.[24] The addition theorem for spherical coordinates determines the following equation [Ref. 24, Eq. (D.14)]:

$$Y_n^m(\theta, \phi) h_n(kr) = \sum_{n'=0}^{\infty} \sum_{m'=-n}^{n} Y_{n'}^{m'}(\theta', \phi') h_{n'}(kr') \beta_{n'm',nm}, \tag{15}$$

where β is defined as

$$\beta_{n'm',nm} = \sum_{n''=0}^{\infty} 4\pi i^{(n'+n''-n)} Y_{n''}^{m-m'}(\theta'', \phi'') \times j_{n''}(kr'')(-1)^m \sqrt{\frac{(2n+1)(2n'+1)(2n''+1)}{4\pi}} \times \begin{pmatrix} n & n' & n'' \\ 0 & 0 & 0 \end{pmatrix} \begin{pmatrix} n & n' & n'' \\ -m & m' & m-m' \end{pmatrix}. \tag{16}$$

Equation (16) has been presented for the case $r' > r''$, which represents the case for which the translation is relatively small compared to the radius of the measurement sphere. Here,

$$\begin{pmatrix} j_1 & j_2 & j_3 \\ m_1 & m_2 & m_3 \end{pmatrix}$$

is the Wigner 3-j symbol.[24] In order to represent the sum in Eq. (15) in a matrix form, the sum is truncated at $n = N$ and a matrix form of the equation can be derived,

$$\mathbf{H} = \mathbf{H}'\mathbf{B}, \tag{17}$$

where matrix $\mathbf{B}$ of size $(N+1)^2 \times (N+1)^2$ is defined by

$$\mathbf{B} = \begin{bmatrix} \beta_{00,00} & \beta_{1-1,00} & \beta_{10,00} & \cdots & \beta_{NN,00} \\ \beta_{00,1-1} & \beta_{1-1,1-1} & \beta_{10,1-1} & \cdots & \beta_{NN,1-1} \\ \vdots & \vdots & \vdots & \ddots & \vdots \\ \beta_{00,NN} & \beta_{1-1,NN} & \beta_{10,NN} & \cdots & \beta_{NN,NN} \end{bmatrix} \tag{18}$$

and $\mathbf{H}$, $\mathbf{H}'$ are defined in Sec. IV. Multiplying both sides of Eq. (17) by $\mathbf{H}'^{\dagger}$ yields

$$\mathbf{H}'^{\dagger}\mathbf{H} = \mathbf{B}, \tag{19}$$

which shows that the numerical transformation matrix $\mathbf{T}$ in Eq. (14) is equal to the analytically defined transformation matrix $\mathbf{B}$, within some truncation errors. A further analysis of translation is presented in Sec. VI.

VI. ERROR ANALYSIS

In this section, errors in the calculation of c_{nm} due to sampling and translation are analyzed. Three types of errors are considered in the process of sound field translation. First, as mentioned in Sec. IV, the matrix $\mathbf{H}$ and the coefficient vector $\mathbf{c}$ are of infinite size. Therefore, a truncation error due to sampling, under the assumption of order-limitation, is unavoidable. Second, the infinite sum in Eq. (15) is truncated, yielding a truncated transformation matrix $\mathbf{T}$. Third, ill-conditioning of $\mathbf{H}$ can cause numerical inaccuracies when calculating $\mathbf{c}$.

A. Sampling truncation error

The first type of error is due to a sampling error and is unavoidable when sampling any function with order higher than the sampling scheme allows. Notwithstanding, if the function decomposition has low amplitudes for high orders, the information loss can be neglected for a high enough order N.

As shown by Rokhlin,[25] if a source satisfies the following expression, named as the radiation condition, for any (θ, ϕ), $c_0 > 0$ and $r \to \infty$:

$$p(r, \theta, \phi) = c_0 \cdot \frac{e^{ikr}}{r} + O\left(\frac{1}{r^2}\right), \tag{20}$$

then there exists $c_0 > 0$ such that for any point located at $r = R$ outside a sphere of radius R_1 surrounding the source, and for $N > kR$,

$$\varepsilon_S \equiv \left| p(k,r,\theta,\phi) - \sum_{n=0}^{N} h_n(kr) \sum_{m=-n}^{n} c_{nm}(k) Y_n^m(\theta,\phi) \right| < c_0 \left(\frac{R_1}{R} \right)^N. \quad (21)$$

There are many physically meaningful pressure functions that satisfy Eq. (20), such as a dislocated monopole or dipole. The left-hand side of Eq. (21) is interpreted as the error between the pressure function and the Hankel expansion, which is bounded on the right-hand side of Eq. (21) by a value that is inversely proportional to the distance from the origin.

By applying the natural logarithm on both sides of Eq. (21) it follows that in order to avoid numerical truncation errors larger than ε_S, the sampling array order N must satisfy

$$N \geq \max \left(kR, \frac{-\ln(\varepsilon_S) + \ln(c_0)}{\ln(R_1) - \ln(R)} \right). \quad (22)$$

However, due to the slow growth of the logarithm function, for sufficiently small c_0 and sufficiently large N it is reasonable to take $N \geq kR$ in order to avoid significant truncation error.

B. Translation truncation error

The second type of error is due to source translation. Equation (15) requires an infinite number of coefficients in order to calculate the translated coefficients without error. For the case of using only a finite number of coefficients a translation truncation error must be considered. We define the translation truncation error as the difference between the pressure function on the measurement sphere, and the spherical harmonics composition of the translated source,

$$\varepsilon_T \equiv \left| p(kr',\Psi') - \sum_{n=0}^{N} h_n(kr') \sum_{m=-n}^{n} c'_{nm}(k) Y_n^m(\Psi') \right| = \left| \sum_{n=N+1}^{\infty} h_n(kr') \sum_{m=-n}^{n} c'_{nm}(k) Y_n^m(\Psi') \right|.$$

If a source is located at the center of a sphere of radius r, and shifted to $\mathbf{r}''$ from the center, then the maximal distance from the measurement sphere surface to the origin is $r + r''$. Using Sec. VI A, the sampling scheme order must satisfy

$$N \geq k(r + r''). \quad (23)$$

Hence, using Eq. (22) for a source with order N_s, the bound on N becomes

$$N \geq N_s + kr''. \quad (24)$$

Based on the work of Coifman *et al.* on the fast multipole method,[26] another bound is given; a source of order N increases its order due to a translation of r'' by

$$L = kr'' + \alpha \ln(kr'' + \pi), \quad (25)$$

where α is a parameter dependent on the desired error ε_T. An empirical experiment[27] shows that $\alpha = 5$ results in a relative error within the range of approximately 10^{-6}. Thus, the translated coefficients should be calculated up to order $L + N$ in order to avoid additional truncation errors due to translation. Assuming the translation is small, the term $\alpha \ln(kr'' + \pi)$ can be neglected so that Eqs. (24) and (25) both lead to the same bound.

For the analytic approach described in Sec. V, if the above-presented condition is met the error due to translation can be neglected. Furthermore, the infinite sum in Eq. (16) does not pose a problem, because the Wigner 3-j symbol is zero for $j_3 > j_1 + j_2$ and therefore the infinite summation (from 0 to ∞) reduces to a finite sum between $\max(|n - n'|, |m - m'|)$ and $n + n'$ and can be computed without truncation error.[28]

For the numerical method this is not the case. In order to compute the transformation matrix $\mathbf{T}$ in Eq. (14) the pseudoinverse of $\mathbf{H}$ is required. Because both $\mathbf{H}$ and $\mathbf{H}'$ are truncated to a finite matrix, an error occurs even for a finite number of coefficients c'_{nm}. Consequently, the analytic approach developed at Sec. V is expected to outperform the numerical approach developed in Sec. IV.

C. Ill-conditioning error

The third type of error is due to ill-conditioning of matrix $\mathbf{H}$. In order to calculate the coefficients c_{nm}, Eq. (9) uses the pseudoinverse of $\mathbf{H}$, so that when the matrix is ill-conditioned the accuracy of the computation can be significantly effected by small numerical or measurements inaccuracies. Ill-conditioning may occur due to the large oscillations of the Hankel functions,[28] but this can be avoided by maintaining the condition $N \lesssim kr$.

Ill-conditioning of $\mathbf{H}$ may therefore occur when the sampling scheme order N is large in relation to kr. When the analyzed frequency is low, this type of error can thus be readily avoided by reducing the effective order of N.

VII. TRANSLATION OF A MONOPOLE SOURCE

Let us consider a simple point source located at the origin as a simple example of translation. The radiated pressure is given by

$$p(k,r,\theta,\phi) = A \frac{e^{ikr}}{r}, \quad (26)$$

where A is the point source amplitude. Using the identity $e^{ikr}/r = ikh_0(kr)$ given in Ref. 16, the spherical harmonics decomposition for a point source will be

$$p(k,r,\theta,\phi) = c_{00}(k) h_0(kr), \quad (27)$$

with $c_{00}(k) = ikA$. From this expression, the coefficient vector for a centralized point source is $c_{nm} = ikA\delta[n]$, where $\delta[\cdot]$ is the Kronecker's δ function. The translated coefficient vector can be computed using the results developed in Sec. V. Multiplying the transformation matrix $\mathbf{B}$ with $\mathbf{c}$ of a point source gives

$$\mathbf{c}'(k) = c_{00}(k) \cdot \mathbf{b} \tag{28}$$

with **b** being the first column of the transformation matrix **B**. Using Eq. (18), the translated coefficient c'_{nm} is equal to

$$c'_{nm}(k) = c_{00}(k)\sqrt{4\pi} j_n(kr'') Y_n^m(\theta'', \phi''). \tag{29}$$

This is the exact computation of the analytic expression for c'_{nm}. Due to the behavior of the spherical Bessel function, c'_{nm} is not limited. This illustrates that a linear translation of an order-limited source may produce an unlimited-order representation. However, for a given kr, the spherical Bessel functions tend to zero as $n \to \infty$, and can be truncated without significant error, as discussed in Sec. VI.

VIII. MEASURES FOR SOURCE ALIGNMENT

In order to align an acoustic source according to its acoustic center, a definition of the acoustic center is required. Both the American National Standards Institute (Ref. 29) and International Electrotechnical Commission (Ref. 30) define the acoustic center in a similar way as the point from which the spherical waves appear to diverge. Rafaely[22] has developed several measures for source alignment that will be presented herein.

When a point source is positioned at the origin, the higher order harmonics are all zero, and thus it is reasonable to look for a source alignment measure that will minimize the energy of the high-order coefficients of c_{nm}. This kind of representation will require the lowest number of coefficients and consequently avoid major truncation errors. Furthermore, this approach leads to an efficient representation, i.e., using the least number of coefficients to represent the source, and thus simplifies spatial audio encoding.

A. The four measures

Based on Ref. 22, four measures for spectral content of the high-order harmonics are presented in this section and are later used as optimization criteria for the performance of source alignment.

(1) J_0—power of the zero-order harmonic,

$$J_0 = 1 - |c_{00}|^2 / L_2, \tag{30}$$

where L_2 is the squared 2-norm of the pressure vector,

$$L_2 = \|\mathbf{c}\|_2^2 = \sum_{n=0}^{N} \sum_{m=-n}^{n} |c_{nm}|^2. \tag{31}$$

(2) J_1—power ratio, extending J_0 to include the first $\bar{N}$ harmonics,

$$J_1 = 1 - \sigma_{\bar{N}}^2 / L_2, \tag{32}$$

where

$$\sigma_{\bar{N}}^2 = \sum_{n=0}^{\bar{N}} \sum_{m=-n}^{n} |c_{nm}|^2 \tag{33}$$

for $\bar{N} < N$.

(3) J_2—center of power,

$$J_2 = \sum_{n=0}^{N} \sum_{m=-n}^{n} n|c_{nm}|^2 / L_2 \tag{34}$$

(4) J_3—center of magnitude.

This measure and J_2 are both inspired by the concept of the center of mass. J_3 is presented and described here for the first time. It is a linear weighting of the absolute value of the coefficients and is defined as

$$J_3 = \sum_{n=0}^{N} \sum_{m=-n}^{n} n|c_{nm}| / L_1, \tag{35}$$

where L_1 is the 1-norm of the coefficients vector,

$$L_1 = \|c\|_1 = \sum_{n=0}^{N} \sum_{m=-n}^{n} |c_{nm}|. \tag{36}$$

J_3 is the first moment of the magnitude of the coefficients. This measure will increase significantly when the moment of c_{nm} is of high order, and conversely, will decrease when it is of low order. Analogous to rigid bodies, when the center of mass is not at the center of the coordinate system, the body is misaligned. On the same note, when the mean harmonic is of high order, the source is misaligned.

B. Measure analysis in a point-source sound field

The value of the four measures for a point source, located at the origin and then translated by a varying distance from 0 to 0.75 of a wavelength, is presented in Fig. 2. Figure 2 shows that J_0 indeed increases with the translation distance, but the variation is not monotonic, and so an optimization approach to find the translation based on J_0 may converge to a local

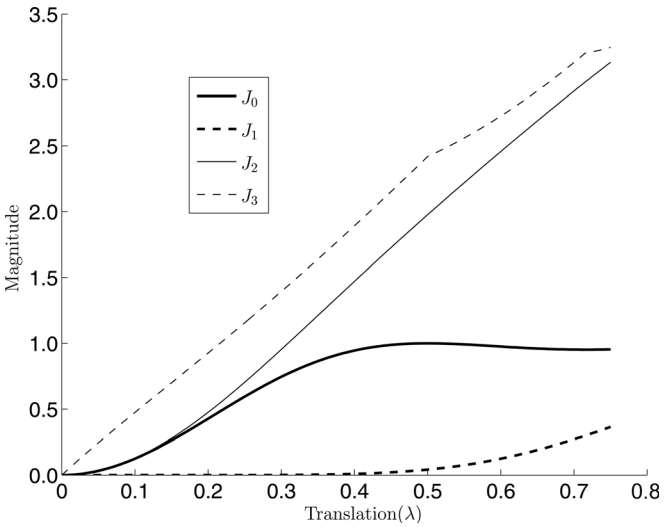

FIG. 2. The values of the four measures J_0, J_1, J_2, and J_3 as defined in Eqs. (30), (32), (34), and (35), respectively, as a function of the translation of a point source.

minimum. Measure J_1 with $\bar{N}=2$ is monotonic, as is J_2, but J_2 is steeper, making potential convergence faster and more robust using J_2 compared to J_1. J_3 achieves the steepest slope, but is not smooth around zero, which may pose a convergence problem for minimization algorithms.

C. The alignment algorithm

The above-presented measures now form the basis for an alignment algorithm. First, a minimization problem is defined as follows:

$$\hat{\mathbf{x}}_i = \arg\min_{x_i} J_i, i = 0, ..., 3, \tag{37}$$

where $\hat{\mathbf{x}}_i$ is the alignment value that minimizes the corresponding measure J_i. Next, an optimization solver is applied to compute $\hat{\mathbf{x}}_i$ in practice. In this paper, the optimization problem is formulated using MATLAB version R2010a, and solved using the built-in function *fminsearch*, which implements the optimization method of the simplex search method.[31]

IX. SIMULATION STUDY

Several simulation examples are presented in this section in order to study the performance of the alignment algorithm. The examples relate to the following sources: (a) a shifted monopole, (b) a monopole and a dipole creating a directional source, and (c) a high-order source. The properties and limitation of the proposed methods will be studied and illustrated through these three examples.

A. Monopole

A monopole source located at $(x, y, z)=(\lambda/10, 0, 0)$ from the origin is surrounded by a spherical microphone array of radius $r=1$ m and order $N=4$, having 100 microphones with an equiangle sampling scheme. For a more detailed description of the spherical microphone array sampling scheme, the reader is referred to Ref. 11. A radiation frequency of $f=125$ Hz is chosen for this example so that $kr=2.29$, in order to illustrate the performance of the alignment algorithm with the different measures, in the case of a low-order source.

The sound pressure is measured at radius $r=1$ m of the origin. The magnitude is plotted in Fig. 3(a), which shows that the sound field for a misaligned monopole is not equal around the sphere. As discussed earlier in Sec. VII, its coefficients c_{nm} are not order-limited, although they do tend to zero as n tends to infinity. This is demonstrated in Fig. 3(c), showing coefficients c_{nm} for $n \leq 4$. The measured pressure at the sphere surface was used as the input to the alignment algorithm. Figure 3(b) shows that after alignment using measure J_2 the sound field is very uniform. Figure 3(c) verifies this showing that $c_{nm} \approx 0$ for every n greater than zero. This indicates that the sound pressure has the same phase and amplitude around the sphere. This result is expected for a monopole located at the origin. Alignment results with the other three measures were similar, with all four measures aligning the source to the origin of the coordinate system, as presented in Table I.

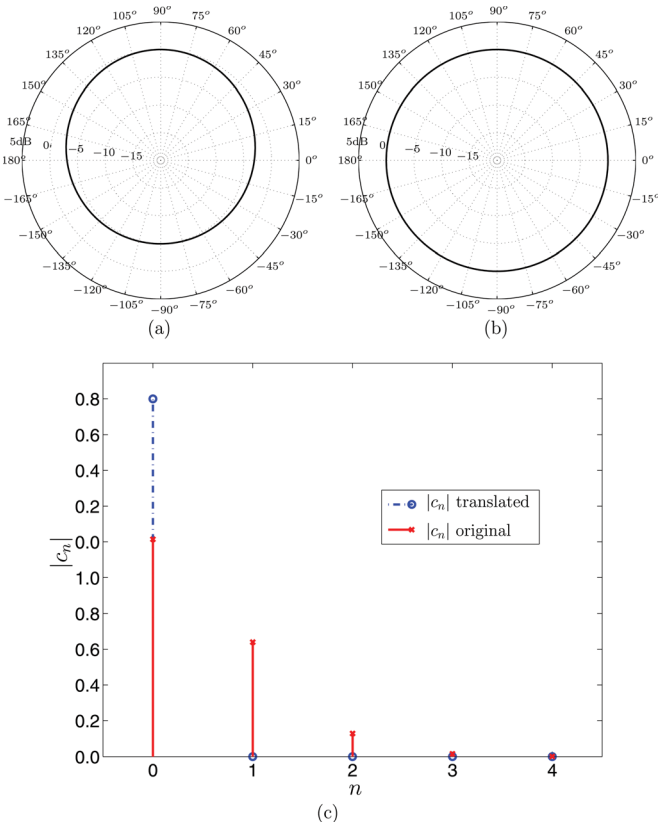

FIG. 3. (Color online) The magnitude of the pressure $|p(kr, \theta, \phi)|$ as a function of the angle θ, for $f=125$ Hz and $\phi=0$ due to a monopole source. (a) At the original position $(x, y, z)=(\lambda/10, 0, 0)$, (b) at the aligned position using the alignment algorithm and J_2, and (c) the coefficients $|c_{nm}|$ of the pressure before and after the alignment.

B. Directional source

The second simulation example employs a directional source, consisting of a weak monopole with a strong dipole component. The source is located $\Delta x=\lambda/10$ m away from the origin along the x axis. This simulation example therefore investigates the performance of the alignment algorithm for highly directional sources.

The setup simulation parameters are the same as in the monopole case, with the pressure at the measurement sphere given by Eq. (4) with $c_{00}=1$, $c_{10}=5$, and $c_{nm}=0$ for all other n, m. Alignment results using measure J_2 are presented in Table II, and Fig. 4. Although the alignment algorithm converged, the alignment position seems to be shifted away from the physical center of the source. Figure 4 shows that

TABLE I. Results of monopole alignment with the four measures.

	x	y	z	Total error
Source location	0.2744	0	0	0
arg min J_0	0.27439	2.7266×10^{-5}	3.6623×10^{-5}	4.7248×10^{-5}
arg min J_1	0.27189	1.322×10^{-5}	-1.8651×10^{-5}	0.0025057
arg min J_2	0.27439	2.7266×10^{-5}	3.6623×10^{-5}	4.7248×10^{-5}
arg min J_3	0.27438	4.1603×10^{-5}	−0.03443	0.03443

TABLE II. Results of directional source alignment with the four measures.

	x	y	z	Total error
Source location	0.2744	0	0	0
arg min J_0	0.27438	-2.3083×10^{-5}	0.81862	0.81862
arg min J_1	0.27442	4.1921×10^{-5}	1.793×10^{-5}	5.1991×10^{-5}
arg min J_2	0.27439	2.6533×10^{-5}	0.65286	0.65286
arg min J_3	0.27442	5.7007×10^{-6}	0.085407	0.085407

the zero-order harmonic has stronger energy compared to all other harmonics, even though most of the original source's energy is in the first harmonic. The alignment value using J_2, which aims to maximize the low-order harmonics and in particular c_{00}, did not match the physical center of the source. For the same reason, alignment values using J_0 and J_3, were different from the physical center. Figures 4(a) and 4(b) show the pressure magnitude as a function of angle θ, before and after alignment, respectively. The dipole-like directivity in Fig. 4(a) is significantly modified in Fig. 4(b), illustrating the effect on sound directivity of alignment to a position away from the physical center.

It is interesting to note that when measure J_1 is used in the alignment algorithm, and the true source order is known, such that $\bar{N}$ can be set to one, the position of the aligned source matches the physical position, as can be seen in Table II. This is as expected because in this case the coefficients of orders higher than one, which appear due to the misalignment, are minimized, therefore producing perfect alignment. This suggests that for non-monopole type sources, J_1 may be preferred if the effective order of the source is known *a priori*. This approach could extend the definition of the acoustic center to sources that have a purely dipolar radiation pattern,[18] and is proposed for further study.

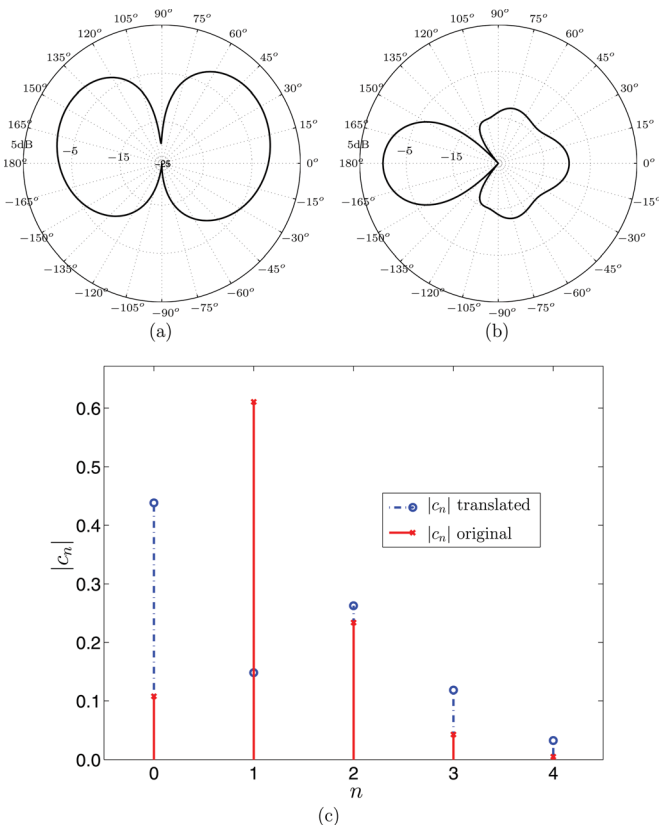

FIG. 4. (Color online) The magnitude of the pressure $|p(kr, \theta, \phi)|$ as a function of the angle θ, for $f = 125$ (Hz) and $\phi = 0$, due to a directional source. (a) At the original position $(x, y, z) = (\lambda/10, 0, 0)$, (b) at the aligned position using the alignment algorithm and J_2, and (c) the coefficients $|c_{nm}|$ of the pressure before and after the alignment.

C. High-order source

The effect of sampling and truncation errors discussed in Sec. VI on the performance of the alignment algorithm is now illustrated. Sampling errors occur when the array sampling order is lower than the source order, and aliasing is expected. In the next simulation, a source with order $N = 6$, with high energy at orders 0 and 6 is considered when displaced by $\Delta x = \lambda/10$ m from the origin. The sound field is sampled using two sampling configurations; first based on an array of order $N = 7$, which is sufficient for sampling the sound field due to a translated source without sampling errors for limited translation values and second based on an array of order $N = 4$, where significant aliasing and truncation errors are expected.

The alignment results are presented in Fig. 5. For the case of the array of order $N = 7$, the alignment algorithm using measure J_2 converged along a convex error surface, with a minimum at the correct position, as can be seen in Fig. 5(b). The corresponding radiation pattern after alignment is the same as the source radiation pattern. However, for the case of array order $N = 4$, the coefficients c_{nm} are miscalculated due to aliasing and translation errors. Therefore, the radiation pattern presented in Fig. 5(c) does not represent the true source radiation pattern and the alignment algorithm using measure J_2 did not converge to the correct alignment value. Furthermore, the error surface is not a convex

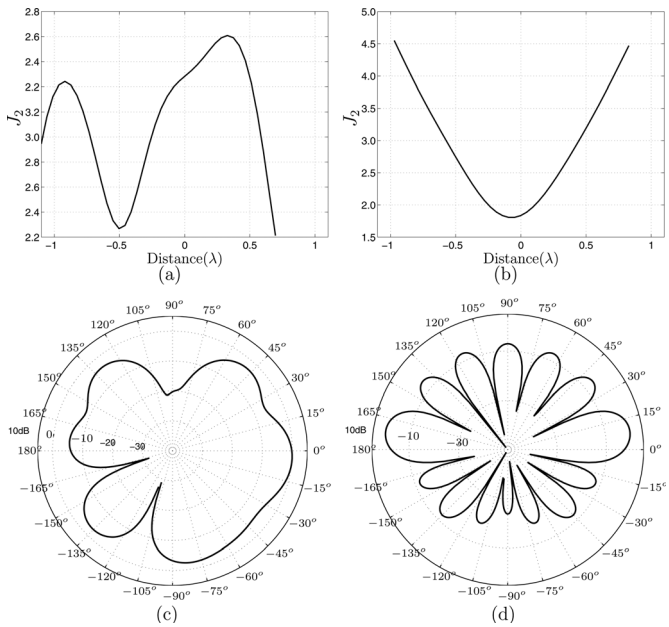

FIG. 5. The measure J_2 due to translation of a source of order $N = 6$ for an array of order $N = 4$ (a) and for an array of order $N = 7$ (b). The magnitude of the pressure $|p(kr, \theta, \phi)|$ and a function of the angle θ, for $f = 125$ (Hz) and $\varphi = 0$ for an array of order $N = 4$ (c) and for an array of order $N = 7$ (d).

function, without a clearly defined minimum within the search range, as can be seen in Fig. 5(a).

X. EXPERIMENTAL STUDY

In order to investigate the proposed methods with real data, recordings of musical instruments were performed with a large surrounding spherical microphone array in a source alignment study. The recordings took place in a full anechoic chamber, as part of a joint project between the Technical University of Berlin and RWTH Aachen University, with the aim of analyzing the natural sound radiation of musical instruments. The instruments were placed inside the microphone array and played chromatic scales, without vibrato or tremolo, during the recording sessions. These recordings are used in the following to investigate the performance of the alignment algorithm with the different measures.

A. Setup

The geometry of the employed microphone array is a truncated icosahedron, with calibrated microphones at the directions of the center points of its 32 faces at a radius of 4.2 m, as described in detail in Ref. 9 and depicted in Fig. 6. The influence of the microphone housings was analyzed with the help of a boundary element method simulation and corrected accordingly.[32] The musicians were positioned facing the positive x axis and having the assumed center of the sound source aligned as accurately as possible with the geometric center of the array. The accuracy of this alignment was limited due to practical constraints. The position of the musician and the musical instruments was documented by two perspective photos, one from the side and one from the front, as can be seen in Fig. 7.

The order of the spherical microphone array used in this experiment is $N=4$, enabling the sampling of an order-limited source with a maximum frequency of 1.1 kHz in order to avoid significant aliasing error. In addition, in order to avoid significant truncation errors when considering translation for a source of orders $N=\{1, 2, 3\}$, a maximal translation of $\{0.67, 0.55, 0.44\}$ m, respectively, is allowed at frequencies lower than 400 Hz.

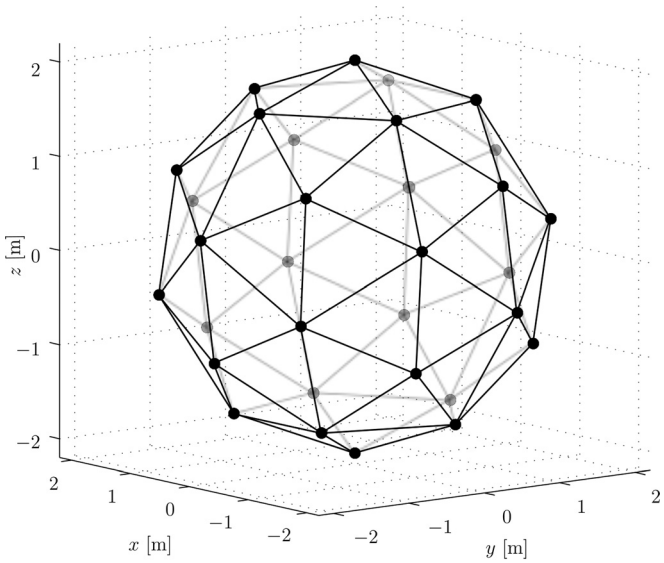

FIG. 6. Geometry of the spherical microphone array used for the directivity recordings (diameter of the array ~4.2 m).

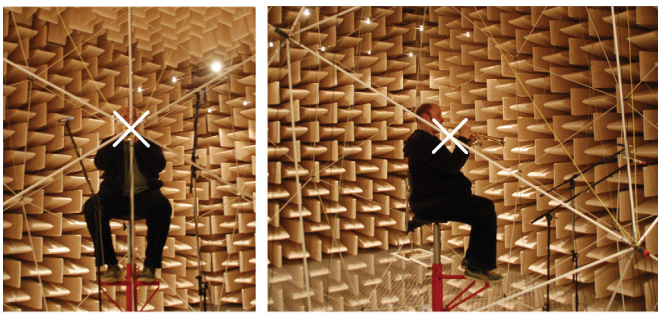

(a) Frontal view (b) Lateral view

FIG. 7. (Color online) Positioning of the trumpet player inside the microphone array. The approximated geometric center of the spherical microphone array is marked with a white cross.

A trumpet was selected as the sound source to investigate the alignment algorithm. The trumpet can be considered as an omnidirectional source at frequencies below 500 Hz, and as a directional source at higher frequencies.[6,33–35] Therefore, the directivity at different frequencies within the operating range of the array may have a different spherical harmonics representation, which may affect the alignment algorithm performance at different frequencies even within the same measurement. Moreover, even though the musician was asked to avoid movement as much as possible, some variance is expected between the different measurements and even during each measurement.

A full scale of the trumpet was recorded at a sampling rate of 44.1 kHz, from the lowest note of F#3 to the highest note of F6, each played for approximately 2 s. The alignment process includes the application of the fast Fourier transform of a size of approximately 88 000 samples for each note. The main harmonics and the alignment of the source are identified using data from each single harmonic using measure J_2, which is the preferred measure for omnidirectional sources, as mentioned previously.

As the goal of this study is the evaluation of the performance of source alignment, the algorithm was applied independently for each harmonic of each played tone. This strategy ensured that the alignment was performed on a single recording each time so that possible errors between several recordings due to movements were minimized. In addition, this facilitated the investigation of the algorithm independently for each frequency.

B. Results

The directivity pattern of the trumpet for several notes, before and after the application of the alignment algorithm, is shown in Fig. 8. One can see that the radiation patterns after translation have smaller ripples, which indicates higher energy at the low harmonic orders. The average reduction in J_2 for all examined notes was about 64%; this supports the results presented in Fig. 8 showing patterns that are assumed to have more significant low-order coefficients.

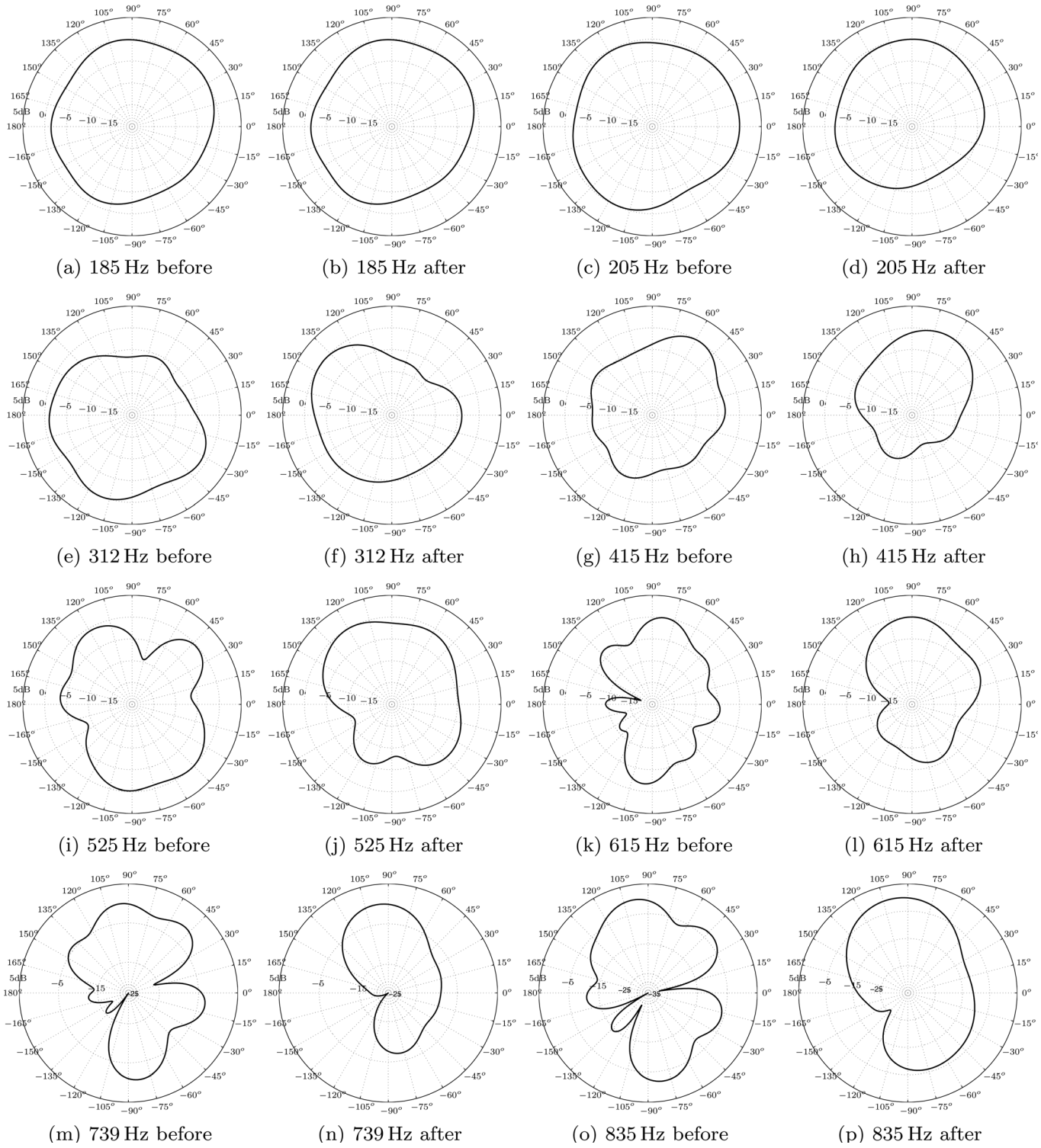

(a) 185 Hz before (b) 185 Hz after (c) 205 Hz before (d) 205 Hz after

(e) 312 Hz before (f) 312 Hz after (g) 415 Hz before (h) 415 Hz after

(i) 525 Hz before (j) 525 Hz after (k) 615 Hz before (l) 615 Hz after

(m) 739 Hz before (n) 739 Hz after (o) 835 Hz before (p) 835 Hz after

FIG. 8. Sound directivity of a trumpet in the horizontal plane before and after translation for several notes.

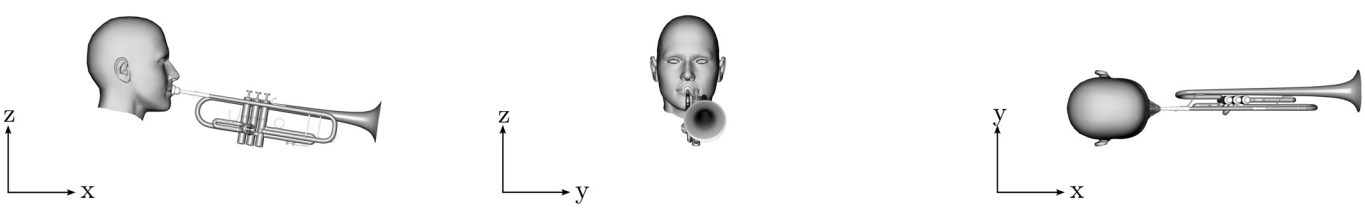

(a) Right view (b) Front view (c) Top view

FIG. 9. An illustration of the axes relative to the musician.

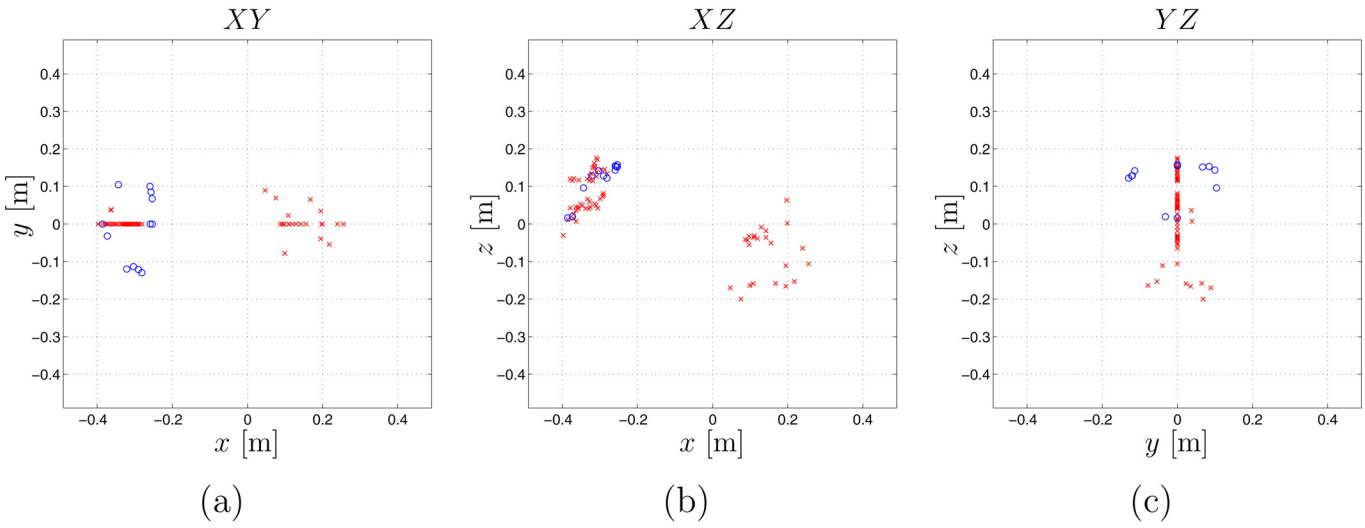

FIG. 10. (Color online) Acoustic centers of trumpet for different notes in XY, XZ, and YZ look directions, computed using the alignment algorithm and J_2. Circlesup to 400Hz, Xs—above 400 Hz.

The algorithm's alignment results are shown in Figs. 9 and in Fig. 10 with each harmonic analyzed separately. The coordinate system is chosen such that the musician is facing the positive x axis, whereas the z axis is pointing upward, as illustrated in Fig. 9. One can see that for low frequencies the results of the algorithm are consistent, showing alignment values around 0.4 m for the xy and xz planes, with a variance of 4.7 mm. For higher frequencies, the variance is 64 mm. This can be explained by the higher order of the source directivity, causing truncation and aliasing errors.

The measure function of criteria J_2 is plotted in Fig. 12 for the note F#4, at a frequency of 370 Hz (fundamental) and 1 100 Hz (second harmonic). For low frequencies the function is convex, thus facilitating correct convergence of the alignment algorithm, while for high frequencies the function is a surface with several local minima. Convergence to the global minimum cannot be guaranteed in this case.

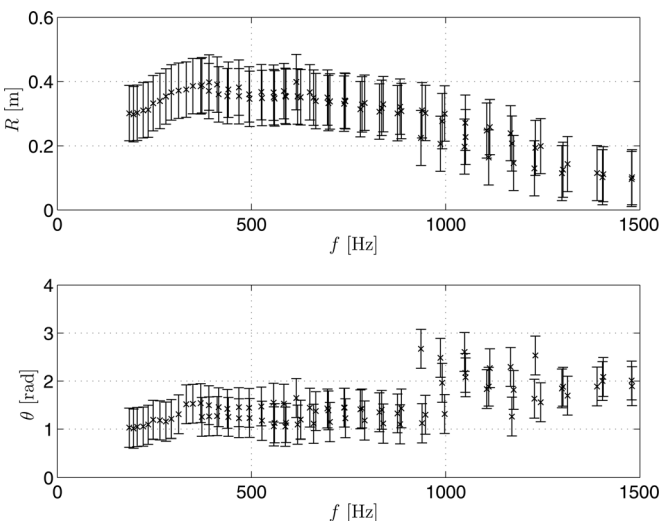

FIG. 11. The radius (upper graph) and angle (lower graph) of the acoustic center of a trumpet for different frequencies. For low frequencies the results are of small variance, and for higher frequencies the results are variable and not consistent.

C. Discussion

When source alignment is performed using measured data the real acoustic center, as a reference value, can approximately be estimated from the perspective photos of the musicians. Therefore, the alignment may be considered successful when the origin, after alignment, is close to the estimated real acoustic center, which is expected when the low harmonics of the measured radiation are more significant. In addition, it is expected that most of the recordings are aligned to the same position, assuming that the musician did not move dramatically during the recording session. For low frequencies, the alignment process exhibits consistent results, and thus achieves compensation of the radiation pattern due to shifting in the source location. In addition, after alignment most of the energy of the source is within the lower orders, and thus the spherical harmonics representation allows a more efficient coding of the radiation pattern. Furthermore, the aligned patterns may be more accurately reproduced when using a spherical sound source as a playback system, since the limited number of loudspeakers only allows controlled reproduction up to a certain order.[36,37] Alignment of sources can thus be useful for spatial coding and auralization purposes.

The setup for the experiment is limited to low frequencies, and achieves good results in the range of up to 400 Hz. It is emphasized that since musical instruments generally cannot produce sound without the musician, we consider the sound source as the instrument together with the musician. Hence, influences such as diffraction off the musician are considered as part of the radiation pattern of the instrument. For higher frequencies there are many factors indicating that the results are not valid; the algorithm converges to distant points for different notes and even for different harmonics of the same note. The error function has more than one minimum, and in some cases the results are too far from the sphere's center to be acceptable. The poor results at higher

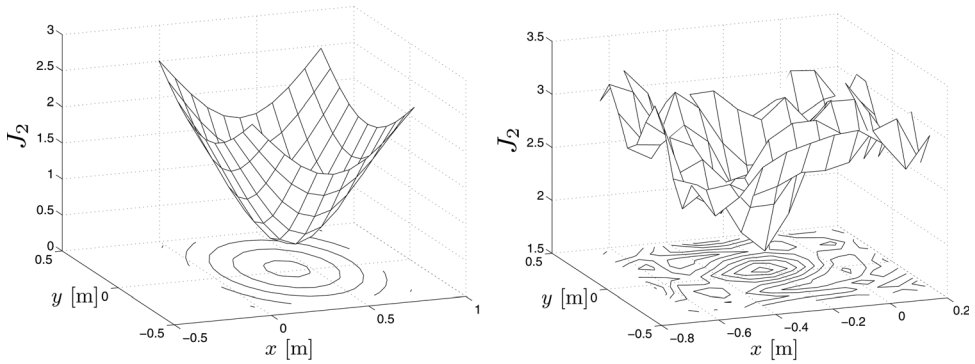

(a) Error function for low frequency (b) Error function for high frequency

FIG. 12. Error function of J_2 criteria (a) for low frequency (370 Hz) and (b) for high frequency (1 100 Hz). For low frequency the source is approximately omnidirectional, and the error function is convex, while for high frequency, the source is directional and the function is not monotonic and has many local minimas.

frequencies can be explained by a few factors. First, as mentioned, the trumpet, as well as many other physical sources, acts as a monopole for lower frequencies. As shown in the simulation study the algorithm performs well for monopole sources, while at higher frequencies the radiation pattern is more directional. Second, the error analysis suggests that the error bounds depend on frequency, and are less confined for higher wave numbers, due to higher kr.

XI. CONCLUSIONS

This paper develops and presents a numerical and an analytical formulation of the spherical harmonics representation of the radiation pattern of a sound source as a function of the translation of the source in the coordinate system. Measures are proposed to reflect the effect of translation on the coefficients of the sound pressure in the spherical harmonics domain. In addition, an extensive error analysis is presented. The proposed algorithm for source alignment has been studied using simulations and experiments. The theory presented here and the measures proposed can be employed for the spatial alignment of acoustic sources in measurements of radiated sound pressure using spherical microphone arrays. Improved measures for directional sources and spatial encoding methods which use this method are proposed for future work.

[1]L. M. Wang and C. B. Burroughs, "Acoustic radiation from bowed violins," J. Acoust. Soc. Am. **110**, 543–555 (2001).

[2]T. Martin and A. Roure, "Optimization of an active noise control system using spherical harmonics expansion of the primary field," J. Sound Vib. **201**, 577–593 (1997).

[3]M. K. Teemu Halkosaari and M. Vaalgamaa, "Directivity of artificial and human speech," J. Audio Eng. Soc. **53**, 620–631 (2005).

[4]F. Bozzoli and A. Farina, "Directivity balloons of real and artificial mouth simulators for measurement of the speech transmission index," in *Audio Engineering Society Convention (AES 115)*, New York, (2003), Vol. 115, p. 5953.

[5]M. Kob and H. Jers, "Directivity measurement of a singer," J. Acoust. Soc. Am. **105**, 1003–1011 (1999).

[6]J. Rindel, F. Otondo, and C. Christensen, "Sound source representation for auralization," in *International Symposium on Room Acoustics: Design and Science* (2004), p. 3862.

[7]J. Štěpánek and Z. Otčenášek, "Sound directivity spectral spaces of violins," in *Proceedings of the International Symposium on Musical Acoustics (ISMA)* (2001), pp. 33–136.

[8]P. Cook and D. Trueman, "Spherical radiation from stringed instruments: Measured, modeled, and reproduced," J. Catgut Acoust. Soc. **3**, 8–14 (1999).

[9]M. Pollow and B. Masiero, "Measuring directivities of natural sound sources with a spherical microphone array," in *Proceedings Ambisonics Symposium*, Graz (2009), pp. 166–169.

[10]F. Hohl, "Kugelmikrofonarray zur Abstrahlungsvermessung von Musikinstrumenten (Spherical microphone array for capturing sound-radiation from musical instruments)," Master's thesis, Institute of Electronic Music and Acoustics, University of Music and Performing Arts, Graz, Austria, 2009.

[11]B. Rafaely, "Analysis and design of spherical microphone arrays," IEEE Trans. Speech Audio Process. **13**, 135–143 (2005).

[12]Z. Li and R. Duraiswami, "Hemispherical microphone arrays for sound capture and beamforming," in *IEEE Workshop on Applications of Signal Processing to Audio and Acoustics (WASPAA 2005)*, New Paltz, New York (2005), pp. 106–109.

[13]M. Park and B. Rafaely, "Sound-field analysis by plane-wave decomposition using spherical microphone array," J. Acoust. Soc. Am. **118**, 3094–3103 (2005).

[14]G. Weinreich and E. B. Arnold, "Method for measuring acoustic radiation fields," J. Acoust. Soc. Am. **68**, 404–411 (1980).

[15]B. Rafaely and M. Kleider, "Spherical microphone array beam steering using Wigner-d weighting," IEEE Signal Process. Lett. **15**, 417–420 (2008).

[16]E. G. Williams, *Fourier Acoustics: Sound Radiation and Nearfield Acoustical Holography* (Academic, New York, 1999), Chap. 6.

[17]F. Jacobsen, S. Figueroa, and K. Rasmussen, "A note on the concept of acoustic center," J. Acoust. Soc. Am. **115**, 1468–1473 (2004).

[18]J. Vanderkooy, "Applications of the acoustic centre," in *Audio Engineering Society Convention (AES 122)*, Vienna, Austria (2007), Vol. 122, p. 7102.

[19]M. Vorländer and H. Bietz, "Novel broad-band reciprocity technique for simultaneous free-field and diffuse-field microphone calibration," Acta Acust. Acust. **80**, 365–377 (1994).

[20]M. S. Ureda, "On the movement of a horn's acoustic center," in *Audio Engineering Society Convention (AES 106)*, Munich, Germany (1999), Vol. 106, p. 4986.

[21]D. Deboy and F. Zotter, "Acoustic center and orientation analysis of sound-radiation recorded with a surrounding spherical microphone array," in *Proceedings of the 2nd International Symposium on Ambisonics and Spherical Acoustics* (2010), p. 21.

[22]B. Rafaely, "Spatial alignment of acoustic sources based on spherical harmonics radiation analysis," in *International Symposium on Control, Communications and Signal Processing (ISCCSP 2010)*, Limassol, Cyprus, 3–5 March 2010, pp. 1–5.

[23]G. Arfken and H. J. Weber, *Mathematical Methods for Physicists*, 6th ed. (Academic, San Diego, 2005), pp. 123–128.

[24]W. C. Chew, *Waves and Fields in Inhomogeneous Media*, 1st ed. (Wiley–IEEE, New York, 1999), pp. 593–599.

[25]V. Rokhlin, "Diagonal forms of translation operators for the Helmholtz equation in three dimensions," Appl. Comput. Harmon. Anal. **1**, 82–93 (1993).

[26]R. Coifman, V. Rokhlin, and S. Wandzura, "The fast multipole method for the wave equation: A pedestrian prescription," IEEE Antennas Propag. Mag. **35**, 7–12 (1993).

[27]J. Song, C.-C. Lu, and W. C. Chew, "Multilevel fast multipole algorithm for electromagnetic scattering by large complex objects," IEEE Trans. Antennas Propag. **45**, 1488–1493 (1997).

[28]S. Koc, J. Song, and W. Chew, "Error analysis for the numerical evaluation of the diagonal forms of the scalar spherical addition theorem," SIAM (Soc. Ind. Appl. Math.) J. Numer. Anal. **36**, 906–921 (1999).

[29]ANSI S1.1-1994: *American Standard Acoustical Terminology, Standards Secretariat* (Acoustical Society of America, New York, 1994).

[30]International Electrotechnical Commission, "Measurement microphones, part 3: Primary methods for free-field calibration of laboratory standard microphones by the reciprocity technique," IEC 61094-3 Ed. 1.0 b:1995 (1995).

[31]J. C. Lagarias, J. A. Reeds, M. H. Wright, and P. E. Wright, "Convergence properties of the Nelder-Mead simplex method in low dimensions," SIAM J. Control Optim. **9**, 112–147 (1998).
[32]M. Pollow, G. K. Behler, and F. Schultz, "Musical instrument recording for building a directivity database," in Fortschritte der Akustik: Tagungsband d. 36. DAGA, Berlin. S.703–704.
[33]F. Otondo, J. Rindel, R. Caussé, N. Misdariis, and P. De la Cuadra, "Directivity of musical instruments in a real performance situation," in *Proceedings of the International Symposium on Musical Acoustics (ISMA)*, Mexico City, Mexico, 6–13 December 2002, pp. 312–318.
[34]J. Meyer, *Acoustics and the Performance of Music: Manual for Acousticians, Audio Engineers, Musicians, Builders of Musical Instruments and Architects* (Springer, Berlin, 2009), pp. 129–177.
[35]H. Olson, *Music, Physics and Engineering* (Dover, New York, 1967), p. 236.
[36]F. Zotter, A. Sontacchi, and R. Höldrich, "Modeling a spherical loudspeaker system as multipole source," Fortschr. Akust. **33**, 221–222 (2007).
[37]M. Pollow and G. K. Behler, "Variable directivity for platonic sound sources based on spherical harmonics optimization," Acta Acust. Acust. **95**, 1082–1092 (2009).